Energy Conversion Circuit Laboratory

Sensor-Reduction Control for SPS-Modulated DAB Converter using Ultra-Local Model

Tan-Quoc Duong[1], *Graduate Student Member, IEEE* and Sung-Jin Choi[2], *Member, IEEE*
[1,2]Department of Electrical, Electronic and Computer Engineering, University of Ulsan, Ulsan, South Korea
Email: [1]duongtanquoc@gmail.com, [2]sjchoi@ulsan.ac.kr

***Abstract*—The most advanced control systems for the dual active bridge (DAB) converter require many high-bandwidth measurement sensors, additional compensation controllers, and sophisticated mathematical calculations. Consequently, cutting down on the total number of sensors and eliminating the need for additional compensation controllers while preserving excellent dynamic performance are considered exciting research areas. Motivated by the abovementioned statements, this paper proposes an ultra-local model-based extended state observer (ESO) strategy for the single phase-shift (SPS)-modulated DAB converter. Because the linear ESO is able to provide accurate measurements of the current, the proposed method eliminates the need for two current sensors on either side of the DAB converter. In addition, only one control parameter is involved in the ultra-local model, which makes developing the controller substantially easier. The viability of the proposed method will be validated by simulations and experiments carried out in various operating circumstances. In addition, the robustness and adaptability of the proposed method will be tested under mismatched parameters.**

Keywords—Sensor-reduction control, Ultra-local model, Extended state observer, Dual active bridge, Single phase-shift.

I. Introduction

In recent years, the dual active bridge (DAB) converter has emerged as a viable topological contender and gained a great deal of scholarly interest due to the merits of galvanic isolation, high voltage conversion gain, and flexible control [1]–[4]. In [4], the authors offered a review of several advanced control methods for controlling the DAB converter, such as feed-forward control [5]–[7], virtual direct power scheme [8], moving discretized control set model predictive control [9]–[12], sliding mode control [13]–[15], etc. However, they require many current and voltage sensors on both the input and output sides of the DAB converter, resulting in a substantial cost and hardware size. In addition, they are complicated and require additional proportional-integral (PI) controllers for compensation.

Obviously, it is necessary to reduce the number of sensors. Besides, the observer control method is regarded as one of the most successful approaches for accomplishing that goal [16]. However, the observer controller also suffers from some problems because it strongly depends on the accuracy of the model and controller gain parameters. On the other hand, the ultra-local model is a workable strategy that can be used to reduce the impact of unknown external factors when applied to various practical situations. In addition, the ultra-local model is a straightforward linear model that is continually kept up to date, and it is designed to account for the absence of knowledge concerning the actual plant model and various kinds of disturbances and uncertainties [17].

By inheriting the merits of the observer and the ultra-local model, this paper offers a linear extended state observer (ESO) strategy for the single phase-shift (SPS)-modulated DAB converter based on the ultra-local model. When compared to other modulation methods, such as dual phase-shift (DPS), extended phase-shift (EPS), and triple phase-shift (TPS), the SPS modulation is regarded as the most simple, straightforward, and is applied the most frequently [1]. As a result, SPS is the modulation utilized to demonstrate the proposed method's effectiveness in this paper. In addition to offering superior dynamic performance, the proposed method does away with the current sensors. In addition, the proposed method does not require any additional PI controller for compensation. Furthermore, the robustness and adaptability of the proposed method to parameter mismatches caused by temperature, aging, and manufacturing tolerance are also taken into account in this paper to show its effectiveness [18], [19].

This paper is organized into four sections. In Section II, the operation principles of the proposed method are presented in detail. In Section III, the simulation and experimental results of the proposed method in various operating situations are shown, and then those results are compared to the existing method's results to demonstrate the effectiveness of the proposed idea. Finally, the conclusions of the paper are presented in Section IV.

II. Operation Principles of The Proposed Method

Fig. 1 shows the typical topology of the DAB converter, consisting of two active bridges coupled by an inductor L and a transformer (turn ratio n:1). C_1 and C_2 are the capacitors responsible for the input and output, respectively. Fig. 2 shows the waveforms of the SPS-modulated DAB converter. D is the phase-shift ratio in the range of [0 ~ 0.5]. Every switch operates at switching frequency f, and the half-switching period is $T_h = T/2 = 1/(2f)$.

It has been demonstrated that the reduced-order model is more effective in complexity and precision than other models, as reported in [4]. Consequently, the reduced-order model will be utilized in this paper to illustrate the proposed idea. The secondary side current i_s and the dynamic equation of the output capacitor C_2 are as follows

$$i_s = \frac{nv_1 D(1-D)}{2fL}, \tag{1}$$

2023 IEEE Applied Power Electronics Conference and Exposition (APEC) | 978-1-6654-7539-6/23/$31.00 ©2023 IEEE | DOI: 10.1109/APEC43580.2023.10131218

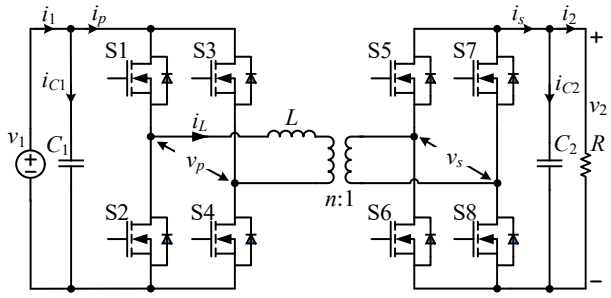

Fig. 1. Topology of the DAB Converter.

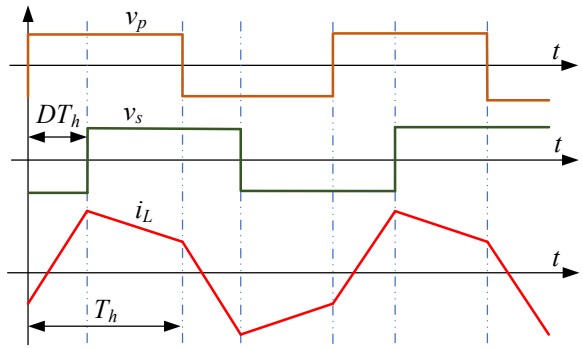

Fig 2. Waveforms of the DAB converter under SPS modulation.

$$\frac{dv_2}{dt}=\frac{i_s-i_2}{C_2}=\frac{nv_1D(1-D)}{2fLC_2}-\frac{i_2}{C_2}. \tag{2}$$

Meanwhile, the first-order ultra-local model of a single-input single-output system is as follows [17]

$$\dot{y}=\alpha u+F, \tag{3}$$

where y and u are the output and control variables, respectively. Constant α represents the input gain, and F is an unknown component that could be continuously updated and represents the system disturbances and uncertainties.

By comparing (2) and (3), the ultra-local model of the SPS-modulated DAB converter can be set up as follows

$$\frac{dv_2}{dt}=\alpha u_D+F, \tag{4}$$

$$\begin{cases}\alpha=\dfrac{nv_1}{2fLC_2},\\ u_D=D(1-D),\\ F=-\dfrac{i_2}{C_2}.\end{cases} \tag{5}$$

Finally, if v_2 and F are regarded as the state variables, a linear ESO is constructed as follows

$$\begin{cases}e_v=z_1-v_2,\\ \dot{z}_1=z_2+\alpha u_D-\beta_1 e_v,\\ \dot{z}_2=-\beta_2 e_v,\end{cases} \tag{6}$$

where $z_1=\hat{v}_2$ and $z_2=\hat{F}$ are the observer values of v_2 and F, respectively [20], [21].

Meanwhile, the characteristic equation of the linear ESO can be deduced as follows

$$\lambda(s)=\left|s\boldsymbol{I}-(\boldsymbol{\Phi}-\boldsymbol{\Psi\Gamma})\right|=s^2+\beta_1 s+\beta_2, \tag{7}$$

$$\begin{cases}\boldsymbol{\Phi}=\begin{bmatrix}0 & 1\\ 0 & 0\end{bmatrix},\\ \boldsymbol{\Gamma}=\begin{bmatrix}1 & 0\end{bmatrix},\\ \boldsymbol{\Psi}=\begin{bmatrix}\beta_1\\ \beta_2\end{bmatrix},\end{cases} \tag{8}$$

where $\boldsymbol{I}$ is the identity matrix, $\beta_1=2\omega_0$, $\beta_2=2\omega_0^2$, and ω_0 is the observer bandwidth [22]–[24].

In order to achieve system stability, robustness, and adaptability, the observer bandwidth ω_0 must be suitably selected. For all simulation and experimental results in this paper, the observer bandwidth ω_0 is selected as 4000 rad/s by considering its inevitable trade-off. When the output voltage $v_2[k+1]$ at the $(k+1)^{th}$ sampling cycle is set to the reference value v_{2ref}, the value of u_D can be calculated from (4) and (6) as follows

$$u_D[k]=\frac{v_2[k+1]-v_2[k]}{T\alpha[k]}-\frac{\hat{F}[k]}{\alpha[k]}=\frac{v_{2ref}-v_2[k]}{T\alpha[k]}-\frac{\hat{F}[k]}{\alpha[k]}. \tag{9}$$

Accordingly, the phase-shift ratio D in the proposed method can be directly obtained as follows

$$D[k]=\frac{1}{2}-\sqrt{\frac{1}{4}-u_D[k]}. \tag{10}$$

Fig. 3 shows the block diagram of the proposed method. Firstly, the value of α is calculated from (5), whereas the observed value $\hat{F}$ is obtained from the linear ESO as expressed in (6). Following that, the value of u_D is calculated based on the constraint expression (9). Finally, the phase-shift ratio D in the proposed method is calculated from (10).

III. Simulation and Experimental Results

In order to demonstrate the effectiveness of the proposed method, the methods to be compared were selected carefully. Since the improved model-based phase-shift (MPS) method presented in [7] has already demonstrated its superior dynamic performance over the conventional PI and MPS methods, simulation and experimental results are only compared to the improved MPS method in this paper. For the purposes of making fair comparisons, the control parameters of both the improved MPS and the proposed methods have been determined to be optimal. The system parameters are shown in Table I.

Fig. 4 shows the simulation results of the two methods under the load current i_2 steps up and down between 1.6 A and 3.2 A when the values of the plant parameters L and C_2

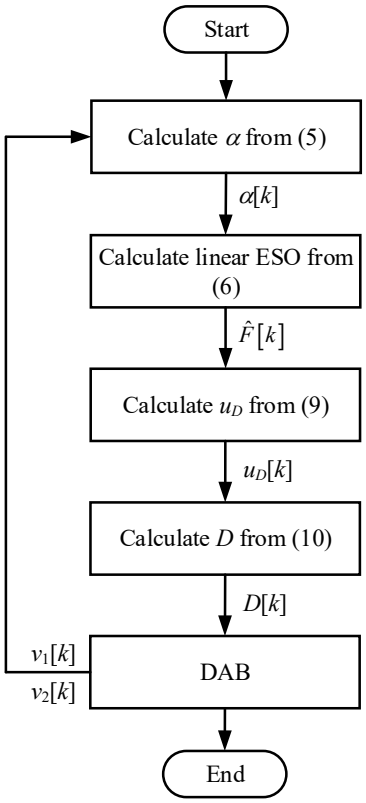

Fig 3. Block diagram of the proposed method.

TABLE I. SYSTEM PARAMETERS

Parameter	Symbol	Value
Input voltage	v_1	100 V
Reference value of the output voltage	v_{2ref}	80 V
Switching frequency	f	10 kHz
Transformer turn ratio	n	1
Inductance	L	50 μH
Input capacitance	C_1	440 μF
Output capacitance	C_2	220 μF

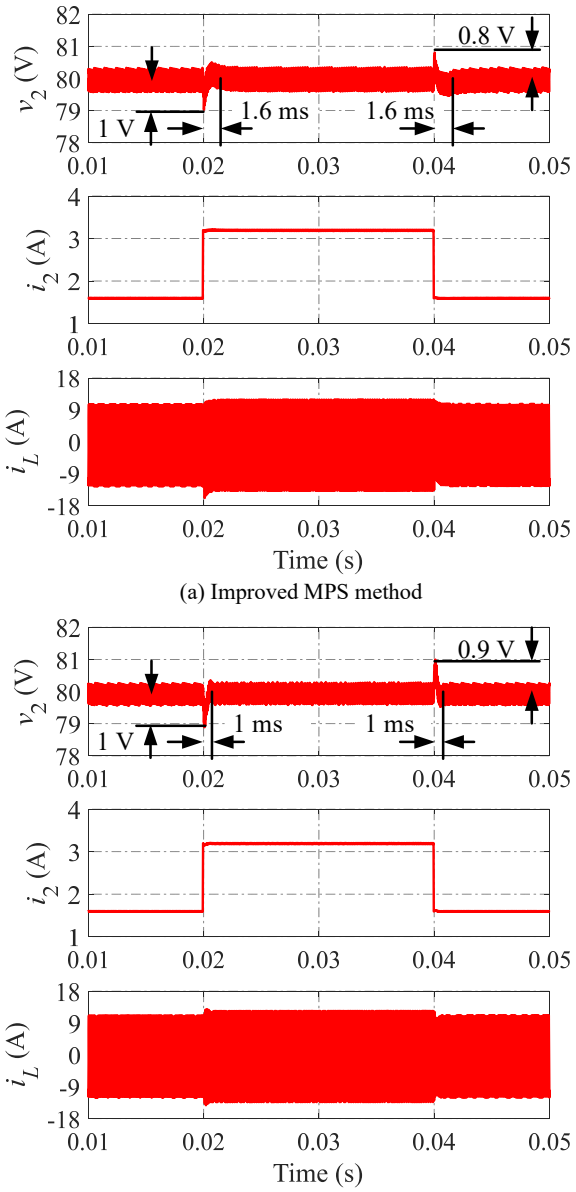

(a) Improved MPS method

(b) Proposed method

Fig. 4. Simulation results under the load current i_2 steps up and down between 1.6 A and 3.2 A when L and C_2 have accurate values.

are accurate. The simulation results are shown in Fig. 5 under the same load current condition when the plant parameters L and C_2 have been mismatched by a 20% increment from the accurate plant values. It is clear that both methods are capable of producing stable output voltages, and their dynamic performances are excellent.

Fig. 6 shows the simulation results of the estimated output current i_{2eso} of the proposed method and the actual output current measured by the sensor $i_{2sensor}$ under the load step change when the output voltage C_2 has mismatched values (Figs. 6(a) and (c)) and accurate value (Fig. 6(b)). Evidently, i_{2eso} and $i_{2sensor}$ are similar in each instance of C_2. This illustrates that the proposed method has excellent observer performance for the load step change. Moreover, this also demonstrates the robustness and adaptability of the proposed method when dealing with parameter mismatches.

Fig. 7 shows the simulation results of the improved MPS method and the proposed method when the reference value v_{2ref} steps up and down between 80 V and 85 V while the values of the plant parameters L and C_2 are accurate. When the output voltage increases, the improved MPS method has a settling time of 2.3 ms, and the overshoot value of v_2 is 1 V. Meanwhile, the settling time is cut down to 1 ms, and the overshoot value of v_2 is brought down to 0.5 V in the proposed method. It is abundantly evident that the proposed method has superior dynamic performance compared to the improved MPS method. Similarly, the effectiveness of the proposed method is also demonstrated in comparison to the improved MPS method when the output voltage decreases. Also, in the proposed method, i_{2eso} and $i_{2sensor}$ are consistent. This proves that the proposed method has excellent observer performance.

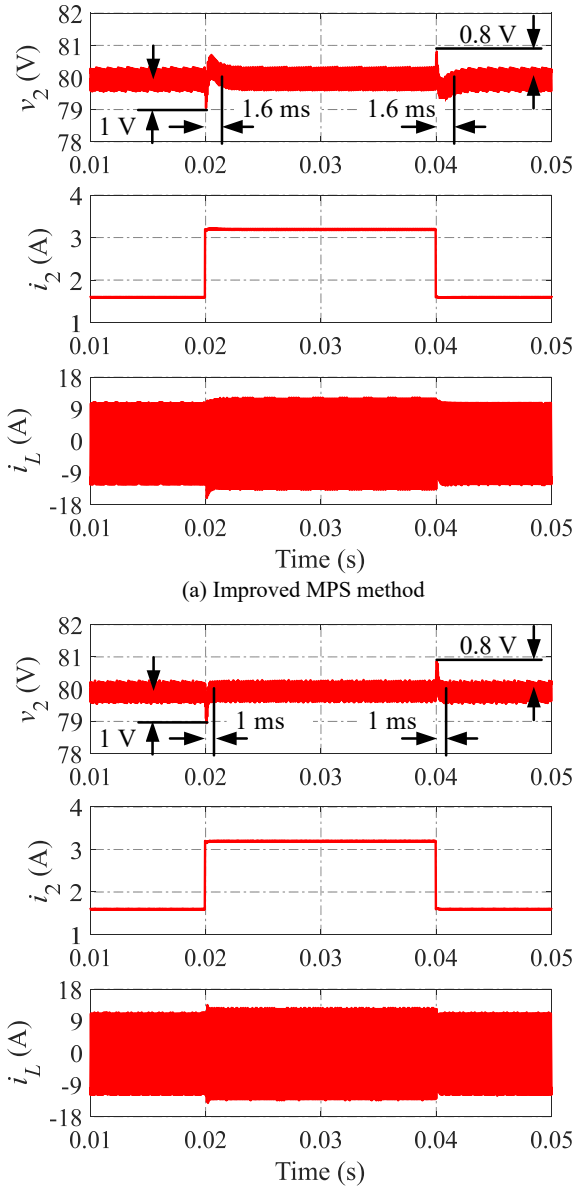

(a) Improved MPS method

(b) Proposed method

Fig. 5. Simulation results under the load current i_2 steps up and down between 1.6 A and 3.2 A when L and C_2 are mismatched by 20% increment.

In order to check the audio-susceptibility, simulation results of the improved MPS method and the proposed method are shown in Fig. 8 when the input voltage v_1 is varied in steps between 100 V and 70 V while the values of the plant parameters L and C_2 are accurate. In this scenario, the improved MPS method has a settling time of 1.5 ms when v_1 is altered. In addition, the overshoot value of v_2 is 0.7 V when v_1 steps down, and the undershoot value of v_2 is 0.9 V when v_1 steps up in the improved MPS method, respectively. Meanwhile, the proposed method has a settling time of 1 ms when v_1 is altered. When v_1 steps down or up, the proposed method has an overshoot and undershoot value of v_2 that is only 0.5 V and 0.6 V, respectively. It is clear that the proposed method demonstrates better dynamic performances compared to the improved MPS method.

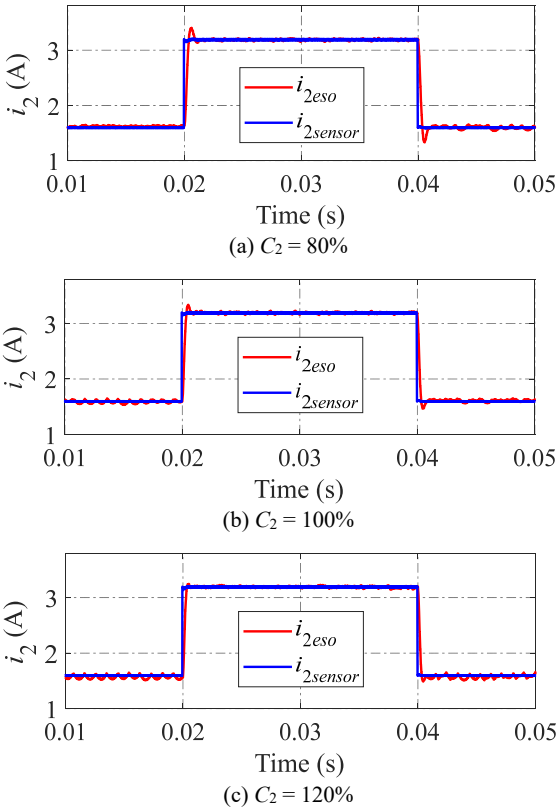

(a) C_2 = 80%

(b) C_2 = 100%

(c) C_2 = 120%

Fig. 6. Comparisons of the estimated output current i_{2eso} and the value measured from the sensor $i_{2sensor}$.

In order to provide additional verification that the simulation results are accurate, an experimental prototype hardware is developed with similar values for all of the system parameters presented in Table I. The experimental results of the improved MPS method are shown in Figs. 9(a) and (b) under the step load current between 1.55 A and 2.3 A when L and C_2 have accurate values. Figs. 9(c) and (d) show the experimental results of the proposed method in the same scenarios. Clearly, the dynamic performances of the output voltage v_2 in both methods are highly similar and excellent, which confirms the simulation results as shown in Fig. 4. In the proposed method, the value of i_{2eso} is entirely consistent with the value of $i_{2sensor}$ in every respect of the load change. This result proves that $i_{2sensor}$ is observed accurately, resulting in an excellent observer performance.

Table II compares the two methods. Two control parameters for the additional PI controller must be designed in the improved MPS method. Meanwhile, in the proposed method, only one control parameter of observer bandwidth needs to be designed. For dynamic performance, the proposed method shows better than the improved MPS method in most operating conditions. Finally, when comparing the number of sensors required in bidirectional mode, it is worth noting that the proposed method eliminates two current sensors, whereas the improved MPS method requires two sensors to measure currents. Obviously, reducing the number of sensors is the most significant advantage of the proposed method compared to the improved MPS method.

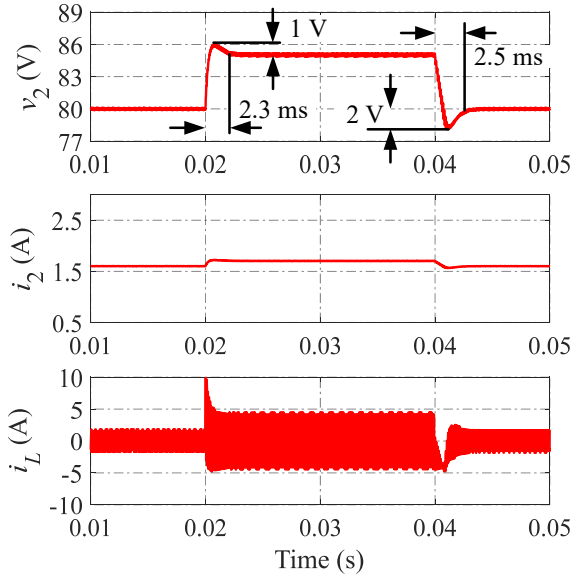

(a) Improved MPS method

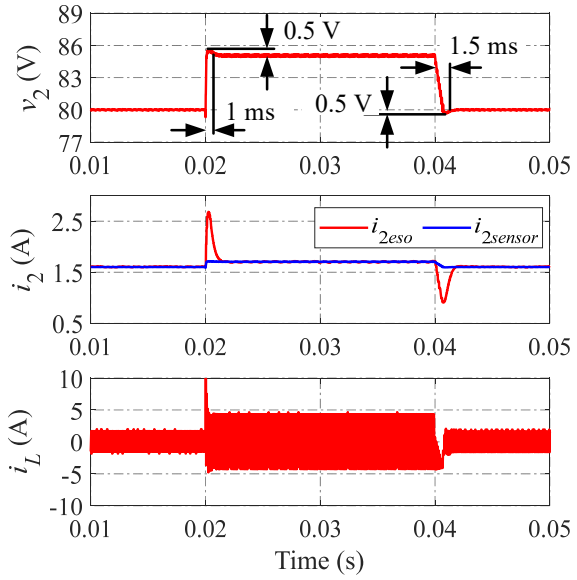

(b) Proposed method

Fig. 7. Simulation results under the reference value v_{2ref} steps up and down between 80 V and 85 V when L and C_2 have accurate values.

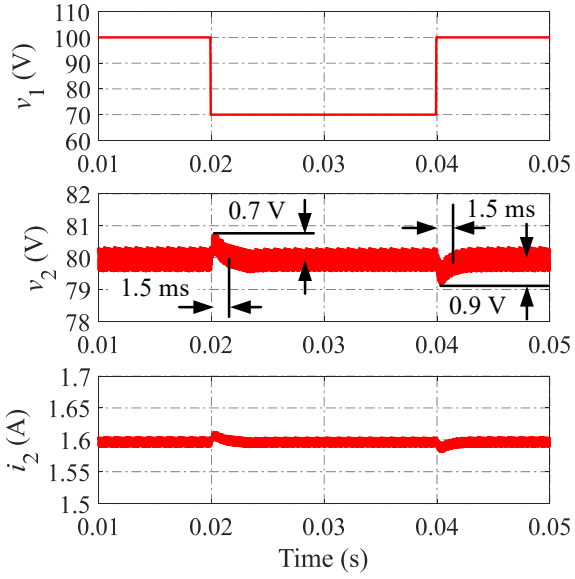

(a) Improved MPS method

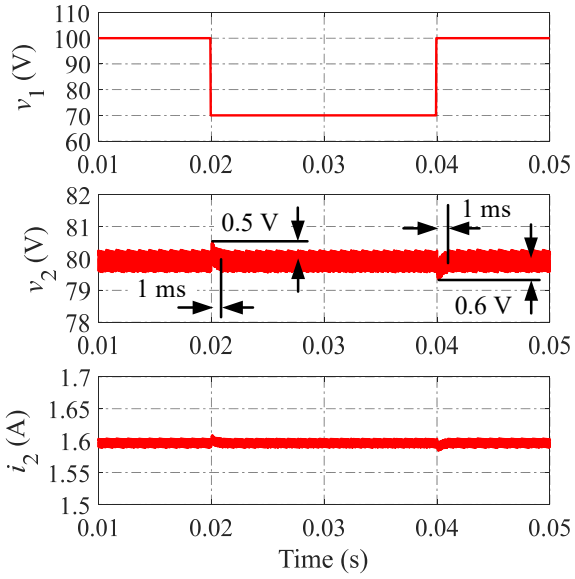

(b) Proposed method

Fig. 8. Simulation results under the input voltage v_1 is varied in steps between 100 V and 70 V when L and C_2 have accurate values.

IV. Conclusions

This paper presented an ultra-local model-based ESO method to reduce the number of sensors for the SPS-modulated DAB converter. Compared to the existing method, the contributions of this paper can be summarized as follows

1. Eliminating two current sensors can reduce system cost and hardware size.
2. The observer bandwidth is the only control parameter that needs to be designed, resulting in a simple controller.
3. The proposed method exhibits excellent observer performance even in the scenarios of circuit parameter mismatch, indicating its robustness and adaptability.

Acknowledgment

This result was supported by Regional Innovation Strategy (RIS) through the National Research Foundation of Korea (NRF), funded by the Ministry of Education (MOE) (2021RIS-003).

References

[1] B. Zhao, Q. Song, W. Liu, and Y. Sun, "Overview of dual-active-bridge isolated bidirectional DC-DC converter for high-frequency-link power-conversion system," *IEEE Trans. Power Electron.*, vol. 29, no. 8, pp. 4091–4106, 2014.

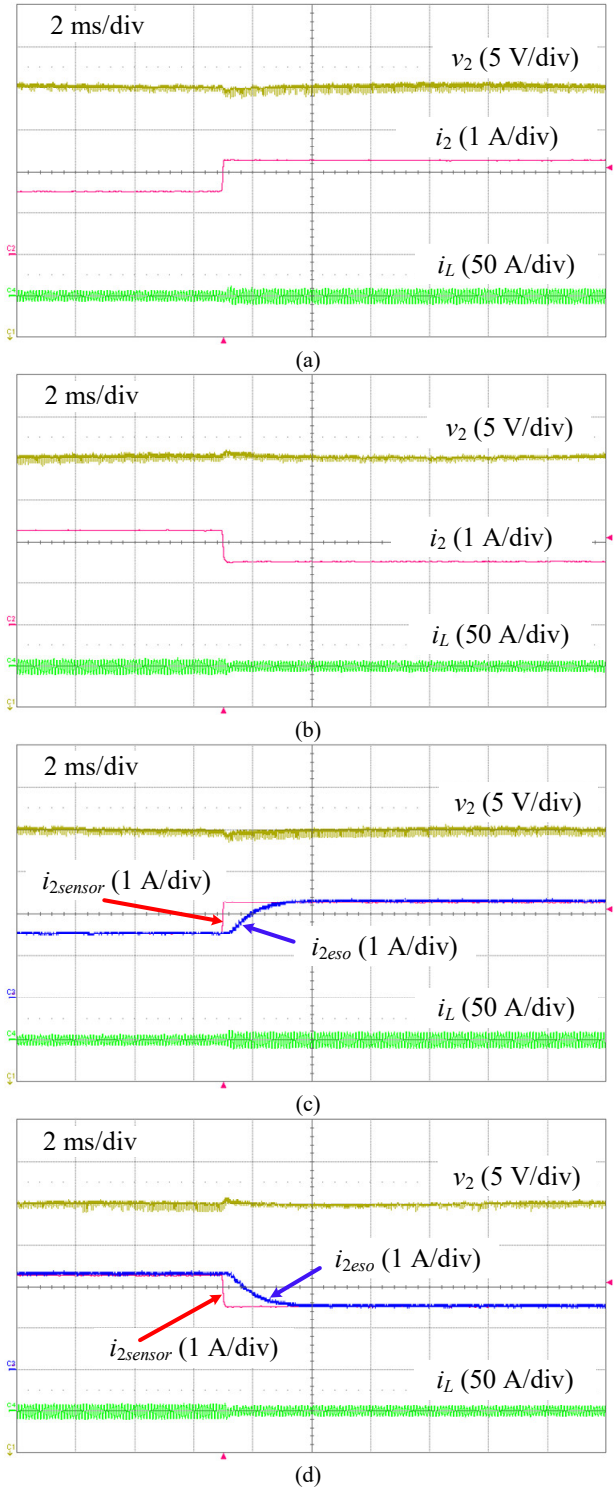

Fig. 9. Experimental results under the step load current when L and C_2 have accurate values. (a) and (b): Improved MPS method; (c) and (d): Proposed method.

TABLE II. SUMMARY COMPARISONS

	Improved MPS method	Proposed method
Control parameters	2 (PI gains)	1 (Observer bandwidth)
Dynamic performance	Good	Excellent
Number of current sensors	2 (i_1 and i_2 sides)	0

[2] N. Hou and Y. W. Li, "Overview and Comparison of Modulation and Control Strategies for a Nonresonant Single-Phase Dual-Active-Bridge DC-DC Converter," *IEEE Trans. Power Electron.*, vol. 35, no. 3, pp. 3148–3172, 2020.

[3] Q. Xu, N. Vafamand, L. Chen, T. Dragicevic, L. Xie, and F. Blaabjerg, "Review on Advanced Control Technologies for Bidirectional DC/DC Converters in DC Microgrids," *IEEE J. Emerg. Sel. Top. Power Electron.*, vol. 9, no. 2, pp. 1205–1221, 2020.

[4] S. Shao *et al.*, "Modeling and Advanced Control of Dual-Active-Bridge DC-DC Converters: A Review," *IEEE Trans. Power Electron.*, vol. 37, no. 2, pp. 1524–1547, 2022.

[5] Z. Shan, J. Jatskevich, H. H. C. Iu, and T. Fernando, "Simplified load-feedforward control design for dual-active-bridge converters with current-mode modulation," *IEEE J. Emerg. Sel. Top. Power Electron.*, vol. 6, no. 4, pp. 2073–2085, 2018.

[6] N. Vazquez and M. Liserre, "Peak current control and feed-forward compensation of a DAB converter," *IEEE Trans. Ind. Electron.*, vol. 67, no. 10, pp. 8381–8391, 2020.

[7] W. Zhao, X. Zhang, S. Gao, and M. Ma, "Improved Model-Based Phase-Shift Control for Fast Dynamic Response of Dual-Active-Bridge," *IEEE J. Emerg. Sel. Top. Power Electron.*, vol. 9, no. 1, pp. 223–231, 2021.

[8] W. Song, N. Hou, and M. Wu, "Virtual Direct Power Control Scheme of Dual Active Bridge DC-DC Converters for Fast Dynamic Response," *IEEE Trans. Power Electron.*, vol. 33, no. 2, pp. 1750–1759, 2018.

[9] L. Chen, S. Shao, Q. Xiao, L. Tarisciotti, P. W. Wheeler, and T. Dragičević, "Model Predictive Control for Dual-Active-Bridge Converters Supplying Pulsed Power Loads in Naval DC Micro-Grids," *IEEE Trans. Power Electron.*, vol. 35, no. 2, pp. 1957–1966, 2020.

[10] L. Chen *et al.*, "Moving discretized control set model-predictive control for dual-active bridge with the triple-phase shift," *IEEE Trans. Power Electron.*, vol. 35, no. 8, pp. 8624–8637, 2020.

[11] Q. Xiao, L. Chen, H. Jia, P. W. Wheeler, and T. Dragicevic, "Model Predictive Control for Dual Active Bridge in Naval DC Microgrids Supplying Pulsed Power Loads Featuring Fast Transition and Online Transformer Current Minimization," *IEEE Trans. Ind. Electron.*, vol. 67, no. 6, pp. 5197–5203, 2020.

[12] L. Chen *et al.*, "Predictive Control Based DC Microgrid Stabilization with the Dual Active Bridge Converter," *IEEE Trans. Ind. Electron.*, vol. 67, no. 10, pp. 8944–8956, 2020.

[13] Y. C. Jeung and D. C. Lee, "Sliding mode control of

bi-directional dual active bridge DC/DC converters for battery energy storage systems," *Conf. Proc. - IEEE Appl. Power Electron. Conf. Expo. - APEC*, pp. 3385–3390, 2017.

[14] N. Tiwary, V. R. Naik N, A. K. Panda, R. K. Lenka, and A. Narendra, "Sliding mode and current observer-based direct power control of dual active bridge converter with constant power load," *Int. Trans. Electr. Energy Syst.*, vol. 31, no. 5, pp. 1–17, 2021.

[15] Y. C. Jeung and D. C. Lee, "Voltage and current regulations of bidirectional isolated dual-active-bridge DC-DC converters based on a double-integral sliding mode control," *IEEE Trans. Power Electron.*, vol. 34, no. 7, pp. 6937–6946, 2019.

[16] D. Sun, "Comments on active disturbance rejection control," *IEEE Trans. Ind. Electron.*, vol. 54, no. 6, pp. 3428–3429, 2007.

[17] M. Fliess and C. Join, "Model-free control," *Int. J. Control*, vol. 86, no. 12, pp. 2228–2252, 2013.

[18] Texas Instruments, "Analog - Passive Devices Application Report," 1999.

[19] P. Wilson, *The Circuit Designer's Companion*, 3rd ed. Newnes, 2012.

[20] S. Zhuo, A. Gaillard, L. Xu, D. Paire, and F. Gao, "Extended State Observer-Based Control of DC-DC Converters for Fuel Cell Application," *IEEE Trans. Power Electron.*, vol. 35, no. 9, pp. 9925–9934, 2020.

[21] T. Q. Duong and S. J. Choi, "Sensor-Reduction Control for Dual Active Bridge Converter Under Dual-Phase-Shift Modulation," *IEEE Access*, vol. 10, pp. 63020–63033, 2022.

[22] C. Zheng, T. Dragicevic, and F. Blaabjerg, "Current-sensorless finite-set model predictive control for LC-Filtered voltage source inverters," *IEEE Trans. Power Electron.*, vol. 35, no. 1, pp. 1086–1095, 2020.

[23] H. Zhang *et al.*, "Extended-State-Observer Based Model Predictive Control of a Hybrid Modular DC Transformer," *IEEE Trans. Ind. Electron.*, vol. 0046, no. 2, pp. 1561–1572, 2022.

[24] Y. Zhang, J. Jin, and L. Huang, "Model-Free Predictive Current Control of PMSM Drives Based on Extended State Observer Using Ultralocal Model," *IEEE Trans. Ind. Electron.*, vol. 68, no. 2, pp. 993–1003, 2021.